(Received 18 June 2025, Accepted 27 August 2025, Scheduled 30 September 2025)

Exploitation of Scattering of VHF Electromagnetic Waves from Jet Engine Exhaust Plasma Formations to Improve Detection Low RCS Aircrafts

Thomas N. Chatziathanasiou, Athanasios Douklias, and Nikolaos Uzunoglu*

Microwave Laboratory, Department of Electrical and Computer Engineering
National Technical University of Athens, Greece

ABSTRACT: The feasibility of utilization of VHF radars, radiating at lower and just above the plasma frequency of the gas formation exhausts of jet engine aircrafts, is investigated as a means to propose anti-stealth detection method. In the first step, the scattering of electromagnetic waves by a plasma sphere is studied, and comparison with Physical Optics (P.O.) Radar Cross Section (RCS) computations is done. This shows the possibility of using P.O. to compute RCS under the assumption of jet engine exhaust plume structured modelled as multilayer prolate spheroid. Also, in the case of radiation frequencies just above the plasma resonance, under the condition of weak scattering — refractive index being close to unity — Rayleigh-Gans approximation is used to compute the RCS. Furthermore, computations based on this model shows the possibility to enhance the RCS of aircrafts by combining the "specular" reflection of part of the exhaust with plasma resonance frequency being higher than the radar frequency and also the part of exhaust having plasma frequency just below the radar radiation frequency. The numerical results show promising mechanisms to compete to improve the detectability of aircrafts with RCS as low as 0,001 m^2.

1. INTRODUCTION

The development of anti-stealth methods has been a challenging issue in the last decades. Several alternative methods have been proposed such as infrared passive receivers detecting radiations from plume formations, multi-static radars and low frequency radars (over the horizon — very high frequency (VHF) and ultra-high frequency (UHF)) [1] and recently microwave radiometry methods [2].

Jet engine exhaust plume formation plasma properties have been studied and are available in the literature [3, 4]. An example case is shown in Fig. 1 where the plume structure is modeled by prolate spheroids having a common "nose" at the nozzle of the engine. In Table 1, the plasma frequencies, dimensions of spheroids and average velocities (with respect to the aircraft) are also shown.

The values computed in Table 1 correspond to modern jet engine aircraft with 80% of its maximum dry engine (military) thrust (without using after burning) with cruising speed flight [5]. This condition was considered realistic in trying to detect a low RCS aircraft. Of course, in the case of maximum thrust, the values given in Table 1 would increase by a factor of 3 to 5 depending on engine characteristics and in particular to nozzle geometry [6]. Such conditions as being transitory in flights (i.e., maneuvers and looping) were considered not important in the present study, aiming to improve the detectability by early warning search radars of cruising low RCS aircrafts. To a second degree, meteorological conditions could affect the plasma characteristics but no more than 10% of the values given in Table 1. Turbulent plasma formations which hold also anisotropy, such as in this case, have been studied by fractional wave functions by the modelling of transport phenomena [7]. Although the multi-spheroid is a simplified model of the very complex exhaust process, the electromagnetic characteristics reserve essential characteristics of the structure allowing to draw conclusions of the backscattering of incident waves emanating from a radar system.

The average velocities are related to Doppler frequencies which could be used to discriminate against the signals returning from plasma formations. This feature could be used by radars with micro-Doppler processing capability to improve the target recognition [8].

2. BACKSCATTERING FROM PLASMA FORMATION OF EXHAUST GASES

To obtain insight to the reflections of electromagnetic waves from a three-dimensional plasma scatterer, consider the case of Fig. 2 of a spherical plasma. Neglecting the collision of electrons with ions phenomena (because of very high frequencies), the dielectric constant of the plasma is [9]:

$$\varepsilon_r(f) = 1 - \frac{f_p^2}{f^2} \tag{1}$$

where f_p is the plasma resonance frequency, and f the radiation frequencies. If $f < f_p$, then ε_r is an imaginary number; if

* Corresponding author: Nikolaos Uzunoglu (nikolaos.uzunoglu@gmail.com).

TABLE 1. Plasma characteristics of exhaust plume of a typical aircraft.

Exhaust plume region i	Plasma Resonance Frequency (MHz) f_{pi}	Minor axis (m) α	Major axis (m) b	Average Velocity (m/s) with respect to aircraft
1	635	0,34	5,18	349
2	280	0,54	9,14	252
3	200	0,68	11,58	228
4	90	0,8	19,82	206
5	63	1,22	27,44	183
6	28	3,36	85,34	160

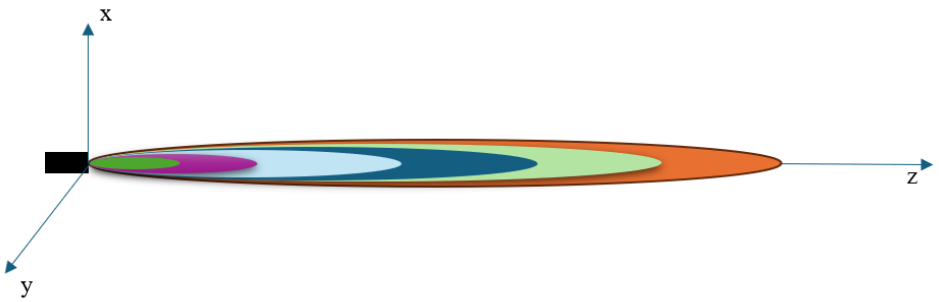

FIGURE 1. Aircraft exhaust plume structure: Each prolate spheroid ($i = 1, 2, 3...$) is characterized with minor (α_i) and major (b_i) axes, plasma frequencies (f_{pi}) depending on the electron densities. All the spheroids "nose" have a common point at the nozzle of the engine.

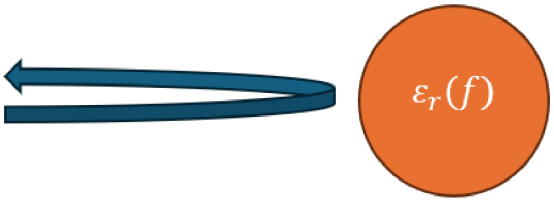

FIGURE 2. Backscattering from a plasma sphere.

$f > 2f_p$, then $\varepsilon_r = 0,75$; as $f \gg f_p$, then $\varepsilon_r \to 1$, and the plasma scatterer disappears.

RCS values were computed, using Mie solution [10], for a plasma sphere at VHF frequencies of two spherical plasma scatter radii $\alpha = 1.25$ and 2.5 meters and plasma resonance frequency $f_p = 280$ MHz, which is a characteristic case of exhaust formations shown in Fig. 1 and Table 1. The results are given in Fig. 3, computed using classical analytic Mie solution. In Fig. 2, the sphere geometry is given. The results show that for various sphere sizes the backscattering becomes strong when $f < f_p$, showing almost a constant value of RCS till $f = 0.2f_p$. If $f > f_p$, the RCS diminishes to a minimum value. Therefore, frequencies $f < f_p$ are suitable for enhance thing RCS. In the present analysis, the collision phenomena between electrons and ions were neglected since the relevant frequencies are less than 10 MHz [5] while the radiation frequencies considered here are higher than 250 MHz. The effect of collision phenomena are negligible because of this fact.

Several recent studies on plasma have been carried out related to the interaction of electromagnetic waves with plasma formation, and the presented mathematical methods could be utilized for further studies [11, 12].

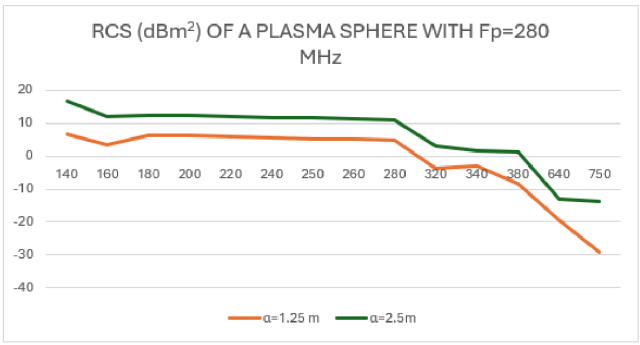

FIGURE 3. Spherical plasma scatterer (horizontal axis MHz, vertical axis RCS (dBm^2).

It is known that in the case of a perfect conductor (PC) spherical scatterer, the physical optics approximation [13] foresees the RCS value

$$\sigma_{\text{PO}} = \pi\alpha^2 \tag{2}$$

Comparing the results in Fig. 3, it is observed that the RCS of the plasma sphere is

$$\sigma_{\text{RCS}} \cong 0,8\sigma_{PO} \tag{3}$$

which is valid when $\frac{2\pi\alpha}{\lambda} \gg 1$, with λ being the radiation wavelength.

Now, considering Eqs. (2) and (3), assuming a prolate spheroid plasma formation, with semi-axes α and b, as shown in Fig. 4 under the condition $f < f_p$, the RCS is computed based on Eq. (3) and physical optics method [14].

$$\sigma_{\text{RCS}} \cong 0,8\frac{\pi b^2}{\left(\sin^2\theta + (b/\alpha)^2\cos^2(\theta)\right)^2} \tag{4}$$

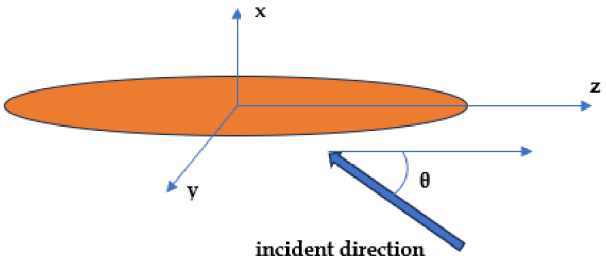

FIGURE 4. Prolate spheroid scatterer.

Then, assuming a radiation frequency $f = 150\,\text{MHz}$, $f_p = 200\,\text{MHz}$ with $\alpha = 0,68\,\text{m}$, $b = 11,58\,\text{m}$ (see Table 1), using Eq. (3), we obtain:

$$\sigma_{\text{RCS}} = \frac{336,85\,(\text{m}^2)}{\left(1 + 289\cos^2(\theta)\right)^2} \tag{5}$$

The electric dimensions of the scatterer with $2\pi\alpha/\lambda = 2.1$ and $2\pi b/\lambda = 36.4$ are in the low edge of the validity of physical optics.

In Fig. 5, the graphic shows the result obtained in Eq. (5) for the RCS of the plume, with an incident angle θ measured from the horizontal axis of the spheroidal plume. According to this approximately 50° angular region with its center of the minor axis of the spheroid, RCS shows $\sigma_{\text{RCS}} > -18\,\text{dBm}^2$. At angles close to the axis of aircraft — either from the front or side-back view at angular ranges 0°–40° (θ) the value of σ_{RCS} is in the range $-25,0$ to $-18\,\text{dBm}^2$. To assess the contribution of plume to total RCS, stealth aircraft skin RCS should be considered at the same VHF region. Considering that the low RCSs of aircrafts [15–17] at VHF frequencies are in average: -23 to $-40\,\text{dBm}^2$, the use of frequencies less than plasma frequency provides a limited marginal anti-stealth capability within the angular region $\theta < 40°$. If the azimuthal angle of the flight axis is close to projection of the incident electromagnetic wave, large differential Doppler shifts exist for the plume scatterer (in present case 353 Hz) and this could help either inbound or outbound direction of the flight, when azimuthal angle is a promising anti-stealth method. As shown in Fig. 6, utilization of the plasma scattering provides limited detection advantages since

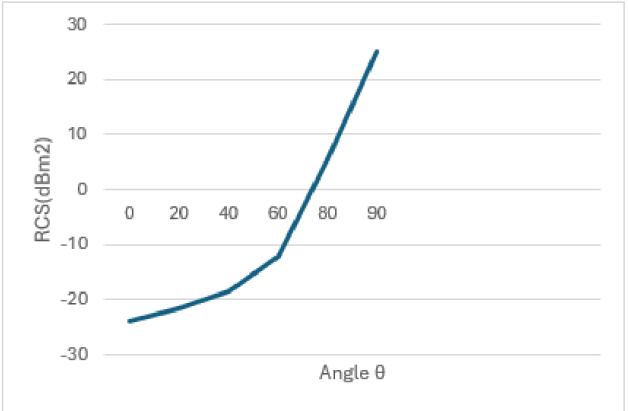

FIGURE 5. Variation of prolate spheroid plasma with angle θ.

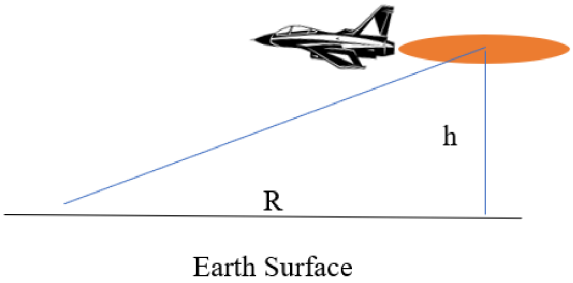

FIGURE 6. Plasma scattering geometry.

if the aircraft flight height is h, the detection range is less than $R < 1,2h$.

3. THE POSSIBILITY OF UTILIZING FREQUENCIES JUST ABOVE THE PLASMA FREQUENCY

In the previous section, the limited anti-stealth capability of using frequencies below the plasma resonance frequency has been shown. As an alternative approach, referring to Fig. 7, the radar frequency f is selected as:

a. If the inner spheroid 1 plasma frequency is $f_{p1} > f$, this region is made non-penetrable to electromagnetic waves.

b. If the frequency f is just above the plasma frequency f_{p2} of the spheroid 2, this region behaves as a medium with a refractive index $n = \sqrt{\varepsilon_r} \leq 1$.

c. If the plasma frequency f_{p3} is $\ll f$, the spheroid 3 has negligible contribution to scattering of electromagnetic waves.

Assuming an incident plane electromagnetic wave to the structure shown in Fig. 7, the scattered field will result in two effects:

a. the polarization currents inside the penetrable spheroid region 2 and

b. the induced surface current in the interface of regions 1 and 2 which is modelled as a perfectly conducting surface.

According to this consideration, at an arbitrary point outside the exhaust structure at far field, the scattered electric field can be written as follows [19]:

$$\mathbf{E}_s(\mathbf{r}) = \frac{\exp(-jk_oR)}{4\pi R}\left[k_o^2\left(n^2-1\right)\iiint_{\substack{\text{Region 2}\\ \text{extracted 1}}} \mathbf{dr}'\right.$$
$$\exp(jk_o\hat{\mathbf{k}}_s\cdot\mathbf{r}')\mathbf{E}_{in}(\mathbf{r}') - j\omega\mu_o\iint_{\substack{\text{Interface}\\ \text{regions 1-2}}} dS'\mathbf{J}_s(\mathbf{r}'_s)$$
$$\left.\exp\left(jk_o\hat{\mathbf{k}}_s\cdot\mathbf{r}'_s\right)\right] \tag{6}$$

where $\hat{\mathbf{k}}_s$ is the unit vector along the scattering direction. Since monostatic RCS is calculated, it is equal to $-\hat{\mathbf{k}}_i$ opposite the incident direction unit vector, and $\mathbf{J}_s$ is the surface current on the interface of regions 1 and 2 spheroids.

In Eq. (1), if $f \geq f_p$, the refractive index is a real number and $n = \sqrt{\varepsilon_r} \leq 1$. Then, the electric field induced inside the spheroid shaped exhaust, being a diaphanous scatterer, can be approximated with the electric field following Rayleigh-Gans approximation [18]:

$$\mathbf{E}_{in}(\mathbf{r}) = \hat{\mathbf{e}}\exp(-jn\mathbf{k}_i\cdot\mathbf{r}) \tag{7}$$

FIGURE 7. Modelling aircraft engine exhaust plasma plume divided into three regions: 1) $f_{p1} > f$ the refractive index being imaginary (high loss medium), 2) $f_{p2} < f$ the refractive index being a real number close to 1 and 3) $f_{p3} \ll f$ the refractive index being very close to 1.

where $\mathbf{k}_i$ is the incident wave propagation vector ($\mathbf{k}_i = k_o\hat{\mathbf{k}}_i$); the free space scalar propagation constant is $\lfloor \mathbf{k}_i \rfloor = k_0$; $\hat{\mathbf{e}}$ is incident wave polarization vector; $\mathbf{r}$ is the position vector inside the exhaust plume.

To compute the RCS with this approximation, first the volume integral in Eq. (6) is computed as the contribution of the "polarization current" inside spheroid 2 (see Fig. 7) before excluding the part of this spheroid occupied by spheroid 1 which is non-penetrable to electromagnetic fields. For the time, neglecting the presence of spheroid 1 and focusing only on spheroid 2, the scattered far field is computed using the equation (first term of Eq. (6)):

$$\mathbf{E}_s(\mathbf{r}) = \hat{\mathbf{e}}\left(n^2-1\right)k_o^2\frac{\exp(-jk_oR)}{4\pi R} \iiint_{\substack{\text{Plume}\\ \text{Volume}}} \mathbf{E}_{in}(\mathbf{r}')\exp\left(-\mathbf{j}\mathbf{k}_i\cdot\mathbf{r}'\right)d\mathbf{r}' \quad (8)$$

Substituting Eq. (7) into (8), using the integral result [19],

$$\iint_{\substack{\text{Spheroid plume}\\ \text{volume}}} \exp\left(-\mathbf{j}\mathbf{P}\cdot\mathbf{r}\right)d\mathbf{r} = 4\pi\alpha^2 b\frac{j_1(\Lambda)}{\Lambda} \quad (9)$$

where α and b are the minor and major axes of a general prolate spheroid, and $j_1(\Lambda)$ is the 1st order spherical Bessel function and

$$\Lambda = \lfloor \mathbf{P} \rfloor \sqrt{\left(b^2\cos^2(\theta_i) + \alpha^2\sin^2(\theta_i)\right)} \quad (10)$$

where:

$$\lfloor \mathbf{P} \rfloor = k_o(1+n) \quad (11)$$

Substituting Eq. (8) into far-field electric vector given in Eq. (7) and substituting the refractive index expression $n^2 = 1-(f_p/f)^2$, after some calculation the following result is obtained

$$E_s(\alpha,b,\omega_p) = \frac{\omega_p^2}{c^2}\frac{\alpha^2 b}{R}\frac{j_1\left(\Lambda(\alpha,b,\omega_p)\right)}{\left(\Lambda(\alpha,b,\omega_p)\right)}\frac{\exp(-jk_oR)}{4\pi R} \quad (12)$$

where $\omega_p = 2\pi f_p$ and E_s is a complex number. Considering the geometry of Fig. 7 and subtracting the inner spheroid which has higher plasma frequency of the radiation frequency and therefore field inside the inner spheroid being strongly attenuated, considering the integration process in Eq. (7), the electric field E_T of the combined spheroids is obtained to be:

$$\mathbf{E}_T = \frac{\omega_p^2}{c^2R}\hat{\mathbf{e}}\left[E_s(\alpha_1,b_1,\omega_p) - \exp(j\psi)\,E_s(\alpha_2,b_2,\omega_p)\right] \quad (13)$$

where α_1, b_1 and α_2, b_2 are the outer (2) and inner (1) spheroids (2) semi-axes (see Fig. 7), while $\exp(j\psi)$ is due to the shift towards the left of spheroid 1 and is

$$\psi = k_0(1+n)(b_2-b_1)\cos(\theta) \quad (14)$$

Now, attention is focused on the second term of Eq. (6), the two-dimensional integral, which is related to the contribution to the scattered field because of the non-penetrable spheroid 1 surface touching spheroid 2. This term corresponds to physical optics contribution already mentioned in previous section and is computed by using stationary phase integration [14]. Considering the coordinate shift and phase term ψ, the result in Eq. (4), of σ_{RCS}, the surface integral contribution E_S can be written as follows:

$$\mathbf{E}_S = \hat{\mathbf{e}}\exp(j\psi)\frac{\exp(-jk_oR)}{4\pi R}\sqrt{\sigma_{\text{RCS}}} \quad (15)$$

Summing up the results of Eqs. (13) and (15), after computing the total electric field $\mathbf{E}_\Sigma = \mathbf{E}_T + \mathbf{E}_S$, the RCS is computed by the definition:

$$\sigma = 4\pi R^2\left|E_\Sigma\right|^2 \text{ as } R\sim\infty \quad (16)$$

4. NUMERICAL RESULTS

Considering the case of plume scatterer with plasma frequency $f_{p2} = 200$ MHz (spheroid 2) and the geometry of the previous Fig. 7, computations were done for $f = 205$ till 250 MHz frequencies. Spheroid 1 has a plasma frequency $f_{p1} = 280$ MHz, and spheroid 3 has a plasma frequency $f_{p3} < 90$ MHz and therefore has negligible effect on incident waves in the frequency band $f = 205$–250 MHz. In Fig. 8, RCS values for the plume scatterer for $f = 205$ till 250 MHz are shown.

At frequencies close to spheroid 2 plasma frequency (205–210), the variation of the RCS with the angle of incidence θ is smooth and above 0 dBm^2. Therefore, the use of frequencies just above the plasma frequency of the intermediate spheroid 2 exhibits strong RCS. Physically this is explainable since at radiation frequencies $f \geq f_{p2}$ the refractive index n of spheroid 2 has values $n = 0.21 \div 0.30$ while at 250 MHz the value of n approaches free space refractive index.

The results of Fig. 8 show that in the case of radar radiation frequency f lower than plasma frequency of "core" region 1 (Fig. 7, $f < f_{p1} = 280$ MHz), while is just above the "coating" region 2 (Fig. 7, $f > f_{p2} = 200$ MHz), the RCS of the exhaust plume shows a "wide" variation with incident angle θ. This means that the exhaust plume at such frequencies shows an enhancement of RCS for all the angles θ and not only when we have a "specular" reflection backscattering which occurs when $\theta = 90°$, that is the radiation incident vertically to plasma

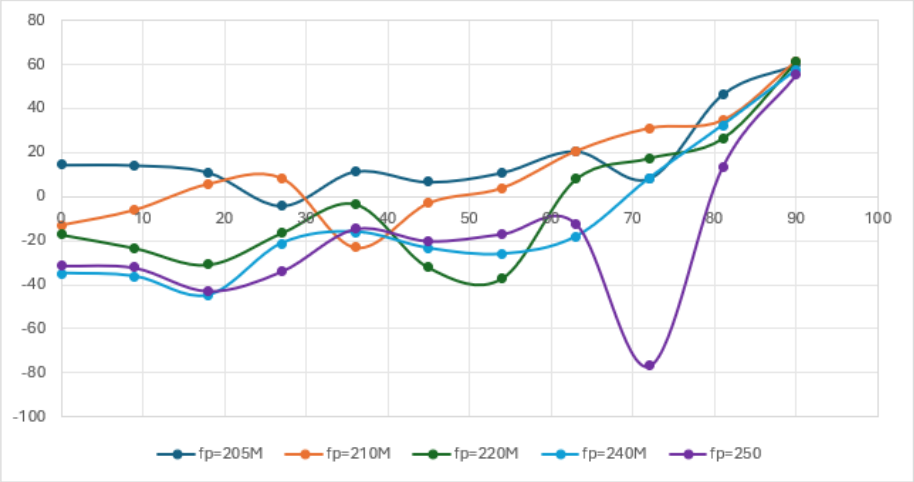

FIGURE 8. Variation RCS values for plume scatterer of Fig. 7 with incident angle θ.

spheroids when the radiation frequency is less than the plasma frequency.

Although it is impossible to know a priori the exact plume regions plasma frequencies for an aircraft to be detected certainly the plasma frequencies will be in the mid VHF frequencies. Considering the above analysis, it can be proposed that a frequency scanning or a multifrequency radar in the spectral region $150 < f < 300$ MHz could be used to detect low RCS aircraft based on the above-mentioned principle. At some frequency, part of the inner volume shows "conductive" behavior, and the "coating" of this volume shows refractive index close to 1, which is shown to exhibit strong RCS for a wide angular region. This method is proposed as an anti-stealth behavior and could be utilized to detect very low RCS jet engine aircrafts. Considering the differential Doppler shifts, it is arguable that the use of VHFs just above the lowest plasma resonance frequency could enhance the RCS of a low RCS aircraft. Since for aircraft cases variations of plasma frequencies will occur but not dramatically, step frequency radar is suitable for the present idea.

It is important to emphasize the fact that the high VHF (30–300 MHz) and low UHF (300–3000 MHz) suggested here to be used in coherent signal processing radars are beneficial also since the atmosphere presents stable propagation conditions not affected by meteorological conditions, and the multipath phenomena are well known and manageable.

5. CONCLUSIONS

The jet aircraft exhaust plume volumes possess inhomogeneous spatial electron densities and as a result an inhomogeneous plasma frequency of the plume. Near the engine nozzle, the plasma frequency is at high VHFs while gradually the plume distancing of the nozzle shows lower plasma frequencies. The possibility of using VHF radar frequencies being less than maximum plasma frequencies (conductive behavior of the core region near nozzle of the engine) while changing frequency to illuminate the main part of the exhaust plume with a frequency just above the plasma frequency shows that a strong RCS behavior is observed for a wide range of illumination angles. This scattering mechanism which combines "specular" type backscattering and "weak" Rayleigh-Gans type scattering provides the opportunity at some frequencies to observe the enhancement of RCS which could be proposed as anti-stealth technique. The possibility of using multi-frequency radars is also possible and most probably the best solution in this endeavor. Since the exhaust plume formation has also an inhomogeneity of the gas velocities, the possibility of using micro-Doppler could also been utilized.

It is noted that the proposed method does not apply to turboprops or other low heat footprint engines. More generally, with this method we try to detect low RCS aircraft. Typically, aircraft using turboprop engines do not have a low RCS, so there is no operational need to apply this method to detect them.

Finally, the present method should be considered as an additional anti-stealth radar technology to other relevant methods such as multi-static radars and detection of infrared radiation from the exhaust gases of aircrafts. However, infrared emissions in 5th generation fighter aircraft have been reduced significantly [20].

REFERENCES

[1] Arvind Dhananjayan, Countering Stealth Technology in Military Aviation, https://indiandefencereview.com/countering-stealth-technology-in-military-aviation/.

[2] Chatziathanasiou, T. N. and N. Uzunoglu, "Theoretical analysis of detection of flying vehicles based on the passive radiometric detection of microwave-millimeter-terahertz wavelength electromagnetic emissions from exhaust plasma gases," *Progress In Electromagnetics Research C*, Vol. 154, 267–275, 2025.

[3] Winther, M. and K. Rypdal, 1.A.3.a, 1.A.5.b Aviation, European Environment Agency, 2017.

[4] Starik, A. M., "Gaseous and particulate emissions with jet engine exhaust and atmospheric pollution," *Advances on Propulsion Technology for High-Speed Aircraft*, Vol. 15, 1–22, 2008.

[5] Technical order 00-105E-9, Revision 11, Chapter 8, Aerospace Emergency Rescue and Mishap Response Information, F-16 aircraft danger areas, Engine Thrusts for F100-PW-229, http://www.0x4d.net/files/AF1/to00-105e-9.htm, 2006.

[6] He, L., Y. Zhang, H. Zeng, and B. Zhao, "Research progress of microwave plasma ignition and assisted combustion," *Chinese Journal of Aeronautics*, Vol. 36, No. 12, 53–76, 2023.

[7] Abu-Shady, M., H. Ahmad, H. Alotaibi, and A. R. Ali, "Investigating the fractional wave function and the impact of topological defects with anisotropic plasma on the dissociation of bottomonium in the fractional non-relativistic quark model," *AIP Advances*, Vol. 14, No. 4, 045011, 2024.

[8] Chen, V. C., D. Tahmoush, and W. J. Miceli, *Radar Micro-Doppler Signatures: Processing and Applications*, IET, 2014.

[9] Stix, T. H., *Waves in Plasmas*, Chapter 1, Springer Science & Business Media, New York, 1992.

[10] Kerker, M., *The Scattering of Light and Other Electromagnetic Radiation*, Elsevier, Jun. 2016.

[11] Yang, X.-J., A. A. Alsolami, and A. R. Ali, "An even entire function of order one is a special solution for a classical wave equation in one-dimensional space," *Thermal Science*, Vol. 27, No. 1B, 491–495, 2023.

[12] Refaie Ali, A., M. N. Alam, and M. W. Parven, "Unveiling optical soliton solutions and bifurcation analysis in the space-time fractional Fokas-Lenells equation via SSE approach," *Scientific Reports*, Vol. 14, No. 1, 2000, 2024.

[13] Crispin, J. W. and K. M. Siegel, *Methods of Radar Cross-Section Analysis*, Chapter 4, Academic Press, New York, 1968.

[14] Trott, K. D., "Stationary phase derivation for RCS of an ellipsoid," *IEEE Antennas and Wireless Propagation Letters*, Vol. 6, 240–243, 2007.

[15] https://militaryembedded.com/radar-ew/signal-processing/radar-cross-section-the-measure-of-stealth (F-22 RCS = 0.0001m2).

[16] https://www.linkedin.com/posts/taits_it-is-amazing-that-an-f35-has-a-smaller-radar-activity-7265068792848756736-NKVU (F-35 RCS = 0.005 m^2, F-117 RCS = 0.003 m^2).

[17] https://www.globalsecurity.org/military/world/stealth-aircraft-rcs.htm (F-35 RCS = 0.005 m^2, F-117 RCS =0.003 m^2, F-22 RCS = 0.0001 m^2).

[18] Jones, D. S., *The Theory of Electromagnetism*, 532, Pergamon Press, Oxford, 1964.

[19] Jahnke, E. and F. Emde, *Tables of Functions*, Chapter VIII, Dover Pub., New York, 1945.

[20] Roy, A. K. and V. S. Karthik, "A critical review of composite materials and stealth technology in modern aerospace engineering," *Int. Jour. of Scientific and Research Publications*, Vol. 14, No. 3, 185–193, Mar. 2024.